Ocean Data Assimilation with Background Error Covariance Derived from OGCM Outputs

FU Weiwei (符伟伟), ZHOU Guangqing* (周广庆), and WANG Huijun (王会军)

Nansen-Zhu International Research Centre (NZC), Institute of Atmospheric Physics, Chinese Academy of Sciences, Beijing 100029

(Received 7 July 2002; revised 26 November 2003)

ABSTRACT

The background error covariance plays an important role in modern data assimilation and analysis systems by determining the spatial spreading of information in the data. A novel method based on model output is proposed to estimate background error covariance for use in Optimum Interpolation. At every model level, anisotropic correlation scales are obtained that give a more detailed description of the spatial correlation structure. Furthermore, the impact of the background field itself is included in the background error covariance. The methodology of the estimation is presented and the structure of the covariance is examined. The results of 20-year assimilation experiments are compared with observations from TOGA–TAO (The Tropical Ocean-Global Atmosphere–Tropical Atmosphere Ocean) array and other analysis data.

Key words: data assimilation, background error, model output, covariance

1. Introduction

Background error covariance plays an important role in a data assimilation or analysis system by determining the distribution of the information from the data in space and between variables (Rabier et al., 1998). An optimal design of background error covariances would ideally reflect the structures of the short-range forecast errors in the assimilation, and modify the increment to yield an analysis field as close to the true values as possible. Therefore, estimation of the background error covariance is very important in data assimilation at present.

Many methods have been developed and applied in operational data assimilation systems over the last few decades. Hollingsworth and Lonnberg (1986) proposed the so-called "observational method", which relies on the use of background departures in an observing network that is dense and large enough to provide information on many scales. Apart from applying the background departure $\mathbf{y} - H[\mathbf{x_b}]$ relating to observations, empirical functions are also adopted to calculate background covariances. Generally, the background error covariances are often obtained as the product of variances and correlation functions. Deber and Rosati (1989) took an empirical formula to calculate the covariances. In their paper, the covariance between any two selected points is given by $ae^{-r^2/(b^2\cos\phi)}$, where ϕ is latitude, r is the horizontal distance of the two selected points, and a and b are empirical parameters and set to 0.01 and 570 km respectively. This formula suggests that the correlation scale decreases from the equator to the poles. Behringer et al. (1998) modified this formula in which b is written as $b^2 = b_{\rm lat}^2 + b_{\rm lon}^2$ denoting the anisotropy in zonal and meridional directions. They also found that the profile of the variance of the temperature correction is proportional to the local profile of $(dT/dz)^{1/2}$. Therefore they assumed a as $a_v \frac{(dT/dz)^{1/2}}{[(dT/dz)^{1/2}]_{\rm b}max}$, where the constant $a_{\rm v}$, is determined empirically. A similar spatial correlation function was also used by others (e.g., Clancy et al., 1990; Meyers et al., 1991). The empirical function can be expressed in other ways. DAO (Data Assimilation Office, 1996) expressed the horizontal correlation by a power-law function $\rho(r) = \left[1 + \frac{1}{2}(\frac{r}{L})\right]^{-1}$, where r is the horizontal distance of any two locations and L is the scale governing the horizontal extent of the correlation. Carton et al. (2000) assumed that the unbiased covariance of two forecast error variables has an exponential form whose weights vary with latitude and depth as well as with their separation. The depen-

*E-mail: zhgq@mail.iap.ac.cn

dence of the horizontal covariance function on depth was constructed to be linear. There are other methods, but fundamentally they fall into three categories: the use of background departure linked with observations, the taking of empirical functions, or the combination of the two.

Estimation of background error covariance by a simple empirical function has its limitations. The "observational method" may be an advisable choice. But problems still exist in the quality of observation because of sparsity in some areas and discontinuity at some intervals, even though the observations have been greatly improved or supplemented by modern measurements. Although the geographical distributions of the typical/dominant spatial and temporal scales are not clear, we note that model output data is homogenous in space and time. Of course, there are some problems with the model output. For example, a bad model will produce output that contains large errors, thus resulting in a poor estimation of background error covariance. The length of the data sequence will affect the estimation of background error covariance. In the tropical ocean, the correlation scales estimated from the data that contains an El Niño process would broaden at the depth of the 20°C isotherm (Meyers et al., 1991). But the problems also exist in observational data. We believe that the grid-point data from a good model record the propagation of information acquired from the initialization and the boundary conditions. Therefore, estimation from the model outputs would physically represent the covariance structure well to some degree. Motivated by such an advantage, we propose a simple method to estimate the covariance. At each level of the model, a Gaussian function is adopted to calculate the covariance between two points, which, in our study, is assumed to vary with longitude, latitude, and the difference in temperature at the previous time step between the two points. The interactions between the vertical levels are not considered. Numerical experiments are designed to verify the new estimation of background error covariance and a great improvement in the analysis fields is shown.

In section 2, the covariance model is described, and the structures of the estimated covariances are presented in section 3. In section 4, results of 20-year numerical experiments are shown to examine the impact of the estimation. A summary and discussion are given in section 5.

2. Covariance model

To obtain optimal estimation of an analyzed field, the following variational problem must be solved (Lorenc, 1986; Deber and Rosati, 1989):

$$J = \frac{1}{2}\boldsymbol{T}^{\mathrm{T}}\boldsymbol{B}^{-1}\boldsymbol{T} + \frac{1}{2}(\boldsymbol{D}(\boldsymbol{T})-\boldsymbol{T}_0)^{\mathrm{T}}\boldsymbol{O}^{-1}(\boldsymbol{D}(\boldsymbol{T})-\boldsymbol{T}_0)\,, \quad (1)$$

where $\boldsymbol{T}$ is an N-component vector containing the correction to the first guess field; $\boldsymbol{B}$ is an estimate of the $N \times N$ background (first guess) error covariance matrix; $\boldsymbol{T}_0$ is an M-component vector containing the innovations, the differences between the observations and the interpolated first guess field; $\boldsymbol{O}$ is an estimate of the $M \times M$ observation error covariance matrix; and $\boldsymbol{D}$ is the observation operator that performs the necessary interpolation and transformation from background space (N) to observation space (M). $(\cdot)^{\mathrm{T}}$ denotes the transpose of $(\cdot)$. The first term on the right-hand side of Eq. (1) measures the fit of differences between the analysis and the background. The second term measures the fit of the differences between the analysis and the observation. The spatial structure and amplitude of the correction field to the first guess or background field are determined by matrix $\boldsymbol{B}$ and $\boldsymbol{O}$ through minimizing J.

The observation errors are assumed to be random and uncorrelated spatially, and thus the matrix $\boldsymbol{O}$ is diagonal. This is not emphasized in the paper. According to Riishøgaard (1998), the $\boldsymbol{B}$-matrix is assumed to be the product of three parts, the standard deviation term, the spatial correlation function, and the correlation induced by the background field itself. The element of $\boldsymbol{B}$ is written as:

$$B_{i,j} = \Lambda_{i,j}\rho_{i,j}(\Delta x, \Delta y)\nu(\theta(T_i)-\theta(T_j))\,, \quad (2)$$

where $\Lambda_{i,j}$ is the product of the standard deviations between any two points i and j which range over the model space, $\rho_{i,j}(\Delta x, \Delta y)$ is a correlation function in which Δx and Δy are the scalar distance in zonal and meridional directions, respectively, between the two points i and j, and $\nu(\theta(T_i)-\theta(T_j))$ represents the difference of the background field itself governing the anisotropy of the background structure where T_i and T_j are the elements of $\boldsymbol{T}$. A Gaussian function is chosen to represent the spatial correlation structure:

$$\rho_{i,j}(\Delta x, \Delta y) = \exp\left(-\frac{\Delta x^2}{L_x^2(x,y,z)} - \frac{\Delta y^2}{L_y^2(x,y,z)}\right)\,. \quad (3)$$

where L_x and L_y are e-folding scales which reflect the extent of spatial correlation, and x, y, and z are model coordinates. It is evident that at each point a pair of L_x and L_y can be acquired by fitting the analytic formula to the scattered points. The scales are estimated as the distance at which the correlation decreases to $1/e$.

In addition to spatial correlation, we consider the impact of the evolution of the background field on the

structure of background error covariance. The underlying idea is that the deformation history of the flow remains embedded in the distribution of the field itself and this would guide the shape of the error correlation. When this term is included in the computation of background error covariance, the structure is tuned to be anisotropic. The basic assumption underlying the use of the anisotropic correlation model is simple: "background errors at nearby points that have similar values of the field are similar" (Riishøgaard, 1998). For thermal-haline circulation, $\theta(\cdot)$ should be a function of temperature along with salinity and surface pressure, but in this study it is simply assumed to be the background field itself, e.g. temperature, $\theta(T) = T$, and

$$\nu(\Delta T) = \exp(-\frac{\Delta T^2}{L_T^2}) \,, \tag{4}$$

where ΔT is the difference of temperature at the two points i and j. It is of the same form as the spatial correlation apart from that it decreases not with the physical distance between two points, but with the difference between the field values themselves (ΔT^2). The impact of this term is that the originally concentric elliptic isolines of the correlation function are distorted towards following the isolines of the background field to some extent. The conjunct correlation will fall off rapidly in the directions in which the field is changing rapidly, while the isotropic correlation will dominate in the direction in which the rate of change of the field is slow. If the scale $L_T \to \infty$, the anisotropic covariance reduces to the isotropic case. The scale of L_T is set to be 5°C empirically in this study.

$\Lambda_{i,j}(x, y, z)$ is thought to be the product of the background unbiased forecast error standard deviation (σ_ε) at two grid points, $\Lambda_{i,j}(x, y, z) = (\sigma_\varepsilon)_i(\sigma_\varepsilon)_j$. In the Kalman filter, background error variance is estimated automatically using the tangent-linear model, so it does not need to be specified. Suppose $z_{j,k}$ is the model estimation at spatial point j and time k, and $x_{j,k}$ is the true value. The relation between $z_{j,k}$ and $x_{j,k}$ is presumed to be:

$$z_{j,k} = x_{j,k} + b_j + \varepsilon_{j,k} \,, \tag{5}$$

where b_j denotes model bias and $\varepsilon_{j,k}$ is the unbiased random forecast error. The background error covariance evolves with time in the Kalman Filter. But for a 3DVar problem, only the stationary part of the background error variance is considered by taking the expectation over time, $\frac{1}{n}\sum_{k=1}^{n}\varepsilon_{j,k}^2$, where n is the number of temporal samples.

Taking the average over time, we can obtain the following formula by assuming that the average of the unbiased random error is zero:

$$\bar{z}_j = \bar{x}_j + b_j, \tag{6}$$

where $\overline{(\cdot)}_j = \frac{1}{n}\sum_{k=1}^{n}(\cdot)_{j,k}$. We approximate the background error variance like this:

$$(\sigma_\varepsilon)_j^2 = \frac{1}{n}\sum_{k=1}^{n}\varepsilon_{j,k}^2 = \frac{1}{n}\sum_{k=1}^{n}(z_{j,k} - x_{j,k} - b_j)^2 \,. \tag{7}$$

The term b_j in Eq. (6) is substituted by that in Eq. (5) to obtain

$$(\sigma_\varepsilon)_j^2 = \frac{1}{n}\sum_{k=1}^{n}[(z_{j,k} - \bar{z}_j) - (x_{j,k} - \bar{x}_j)]^2 \,, \tag{8}$$

where $z_{j,k} - \bar{z}_j$ represents the model-estimated anomaly and $x_{j,k} - \bar{x}_j$ refers to the anomaly of the true value.

Reducing the right-hand side of Eq. (8), we can obtain:

$$(\sigma_\varepsilon)_j^2 = (\sigma_m)_j^2 + (\sigma_t)_j^2 - 2\frac{1}{n}\sum_{k=1}^{n}(z_{j,k} - \bar{z}_j)(x_{j,k} - \bar{x}_j) \,, \tag{9}$$

where

$$(\sigma_m)_j^2 = \frac{1}{n}\sum_{k=1}^{n}(z_{j,k} - \bar{z}_j)^2 \,, \tag{10}$$

$$(\sigma_t)_j^2 = \frac{1}{n}\sum_{k=1}^{n}(x_{j,k} - \bar{x}_j)^2 \,. \tag{11}$$

The third term on the right-hand side of Eq. (9) can be written further as $r_j(\sigma_m)_j(\sigma_T)_j$, where

$$r_j = \frac{\frac{1}{n}\sum_{k=1}^{n}(z_{j,k} - \bar{z}_j)(x_{j,k} - \bar{x}_j)}{(\sigma_m)_j(\sigma_t)_j} \tag{12}$$

is regarded as the correlation between the model estimation and the true value.

Suppose $c_j = (\sigma_t)_j/(\sigma_m)_j$, we obtain

$$(\sigma_\varepsilon)_j^2 = (\sigma_m)_j^2(1 + c_j^2 - 2r_jc_j) \,. \tag{13}$$

Because the observed data are inserted into the model continuously during model integration, it is reasonable to suppose $r_j \approx 1$; then Eq. (13) becomes

$$(\sigma_\varepsilon)_j^2 \approx (\sigma_m)_j^2(1 - c_j)^2 \,. \tag{14}$$

The parameter c_j should vary in space, but in this study it is assumed to be a constant. Also because of the continuous insertion of observed data, c_j should be close to 1; then $0.5 \leqslant c_j \leqslant 1.5$ is a reasonable estimation. So $(1 - c_j)^2$ is set to 0.25 in this study.

The process indicates that the background error covariance in our study is estimated as a part of the covariance of the modeled variations. One advantage of this is to avoid the estimation of model error directly since the oceanic model errors depend not only on the model itself but also on the atmospheric forcing

errors (Zhu and Kamachi, 2000), which are difficult to specify.

3. Estimating error covariances

3.1 *Dynamic model*

The oceanic numerical model used in this study is a tropical Pacific general circulation model developed by Zhang and Endoh (1992). This model is a part of the ENSO prediction system at the Institute of Atmospheric Physics, the Chinese Academy of Sciences (IAP/CAS) (Zhou et al., 1999; Zhou and Zeng, 2001). The dynamics of the model are governed by the primitive equations under hydrostatics and the Boussinesq approximation. The model removes the constraint of "rigid lid" in that the sea surface is set to be free. In the horizontal, a staggered $2°\times1°$ longitude-latitude grid is used in the tropical Pacific Ocean domain (30°N–30°S, 121°E–69°W). The vertical resolution is 14 levels, with 10 levels between the surface and 240 m depth. The model includes the convective adjustment procedure when hydrostatical unstability occurs. The lateral boundaries are set to be "non-fli" and "non-flux", but at the north and south boundaries, the relaxation terms $\gamma(T^*–T)$ and $\gamma(S^*–S)$ are included in the $T-S$ equations, where T and S represent temperature and salinity respectively, γ is the Newton cooling coefficient, which equals $(60\,\mathrm{d})^{-1}$, and T^* and S^* are the climatologies of Levitus (1982).

In this study, the oceanic model was forced by wind stress anomaly product from the surface marine report at Florida State University (FSU) (Bourassa et al., 2001) blended with the climatologies of Hellerman and Rosenstein (1983) and sea surface temperature (SST) (Reynolds and Smith, 1994) as the relaxation of heat flux. The impact of fresh water was ignored. The model was integrated from 1978 to 2002 from the initial condition of the model climatology. Monthly mean outputs of the model at every space point were saved as the control run and used to estimate the background error variances and correlation scales.

3.2 *Structures of the estimations*

L_x and L_y are calculated at each level of the model as follows: the data pairs of temperature are formed by subtracting the average over time from its temperature at each grid point. The set of data pairs is then used to compute the correlation coefficient between different grid points. Calculation of the fitting is performed via a nonlinear fit procedure. Considering that correlations far from the calculated point are found to be too noisy to produce stable statistics, only data within a $20°\times20°$ bin are chosen. In some cases, the function is so flat that the e-folding value is not found. In these cases, L_x and L_y are set to 2400 km and 700 km respectively. The fits of the zonal and meridional scales at the surface (10 m in the model) on the equator and in the subtropics are shown in Fig. 1.

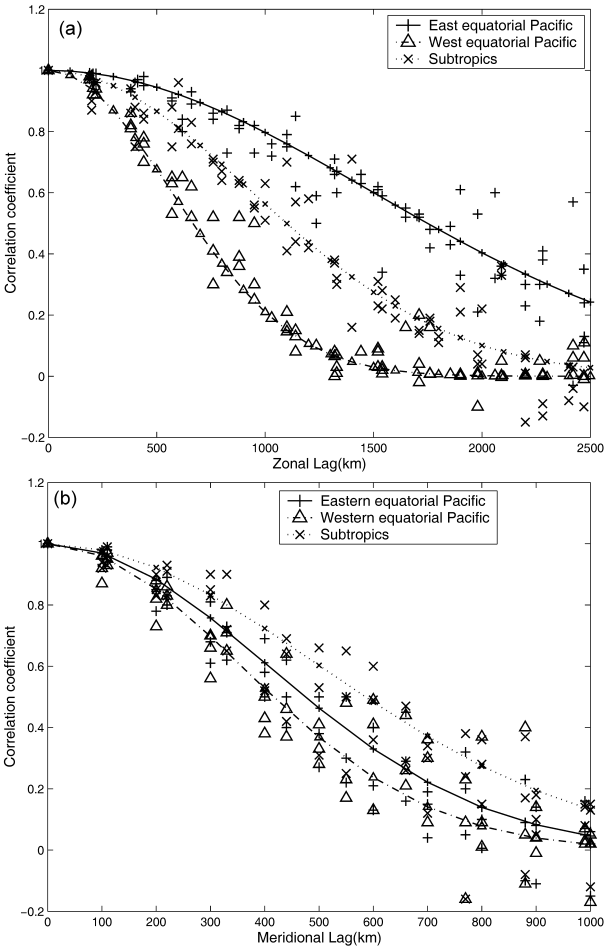

Fig. 1. Correlation coefficient as a function of lag distance in three areas: (a) for zonal scales, and (b) for meridianal scales. The solid line is for eastern equatorial Pacific, the dashed line is for western equatorial Pacific, and the dotted line is for midlatitudes. The distance where the correlation coefficient decreases to $1/e$ shows the desired correlation scale.

Figures 2 and 3 show the distribution of the spatial correlation scales in the zonal and meridional directions, respectively. The distribution of the zonal correlation scale from the equator to 30°N(S) at the sea surface (10-m depth in the model layer) exhibits an asymmetric character (Fig. 2a). In the region between 5°N and 5°S, the large values are located in the eastern equatorial Pacific with the maximum value above 2000 km, while the western equatorial Pacific is a lower-value area where the minimum is below 800 km. This

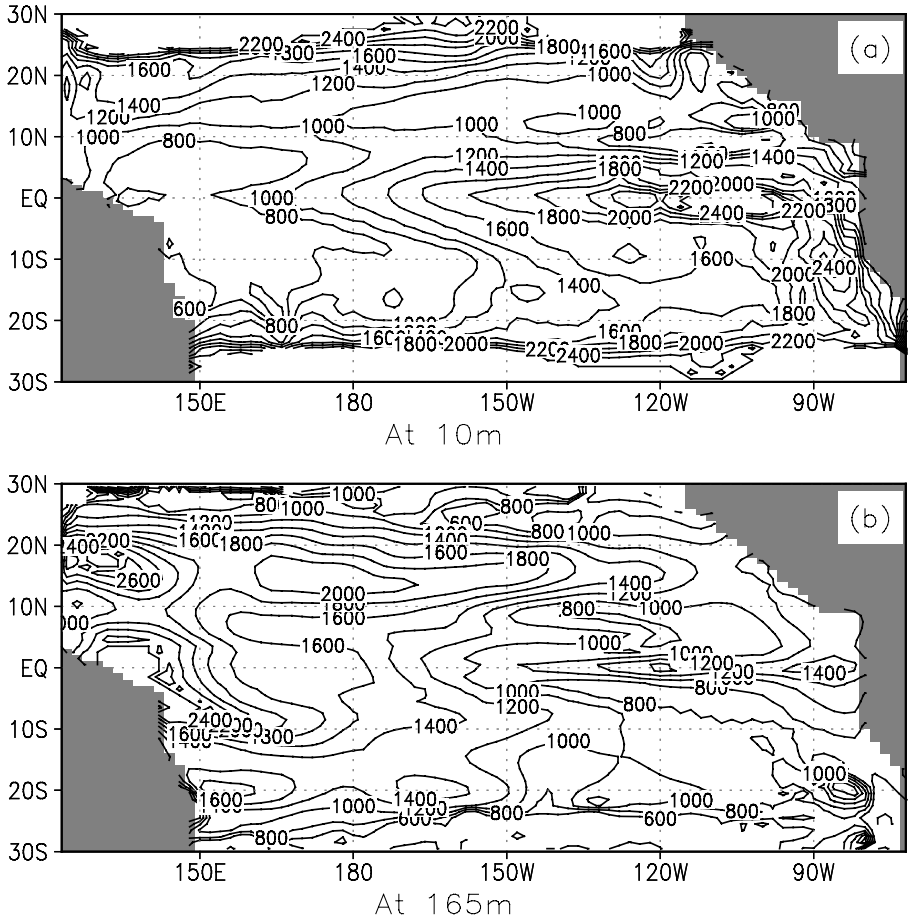

Fig. 2. Distribution of the zonal correlation scales at (a) surface (10 m in the model), (b) 165 m. The contour interval is 200 km.

is probably associated with the equatorial wave guide in the band of 5°N and 5°S where the zonal current in the central and eastern Pacific is much larger than in the western Pacific. From 5°N to 10°N, the zonal correlation scale decreases rapidly in the eastern Pacific where the westward South Equatorial Current (SEC) reverses gradually to the eastward North Equatorial Countercurrent (NECC). The relatively smaller zonal scale band between 10°N and 20°N corresponds to the North Equatorial Current (NEC) which was rather weak in the simulation compared to the observation (Zhang and Endoh, 1992). The correlation scales increase to values above 2000 km in the whole basin of the ocean from 20°N to the middle latitudes associated with the North Pacific Current.

In the South Pacific, the structure of the zonal correlation scale is relatively simple, where a small-value band extends from the western Pacific to the central tropical Pacific in a south-eastward direction. In the western tropical Pacific, the small scale may be due to the weak and complicated current structure in this area. Our results are comparable to those of McPhaden and Taft (1988), who also showed the zonal correlation scales with the values of 15–20° longitudinal degrees along the equator in the eastern Pacific. Their results were acquired from moored time series data.

The zonal correlation scales at a depth of 75 m are similar to or smaller than that of the surface in most areas (figure not given). However, at a depth of 165 m, the distribution of correlation scales differs greatly from that of the surface. In the western Pacific between 20°N–10°S, the zonal correlation scales dramatically increase, showing a maximum over 2400 km near the equator and 18°N. Other than the increasing trend from the equator to 30°N(S) in the surface, the scales basically display a decreasing trend in this region. In the eastern equatorial Pacific, the large-value band along the equator becomes narrow with the maximum value decreasing, and the lower-value region moves somewhat to the equator which is around 10°N at the surface. The scales in the band of 10°N to 20°N

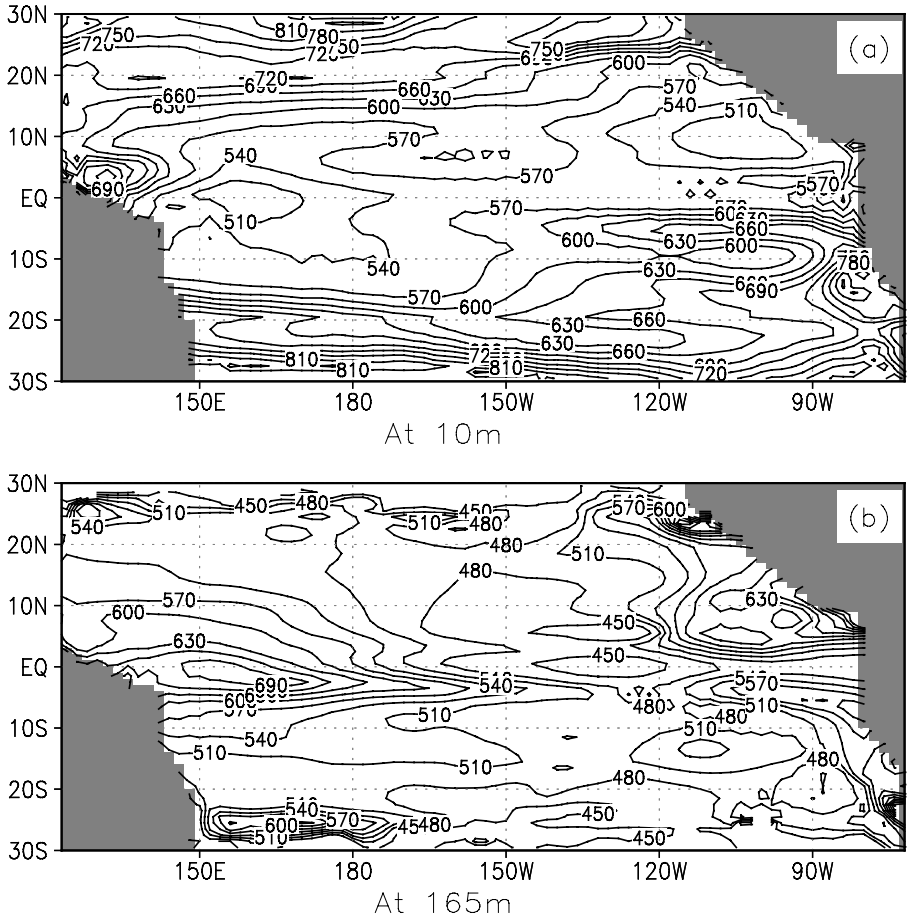

Fig. 3. Same as Fig. 2 but for the meridional correlation scales. The contour interval is 30 km.

Table 1. Comparison of meridional correlation scales (φ) and standard deviations (σ) in the tropical Pacific between Meyers et al.'s results (1991) and our estimation.

	New Caledonia–Japan				New Caledonia–Hawaii				Tahiti–Panama			
	Meyers et al.		the model		Meyers et al.		the model		Meyers et al.		the model	
	φ (°lat)	σ (°C)	φ (°lat)	σ (°C)	φ (°lat)	σ (°C)	φ (°lat)	σ (°C)	φ (°lat)	σ (°C)	φ (°lat)	σ (°C)
18°N	6.0	1.1	6.1	1.1	6.0	1.0	5.4	1.0				
15°N	6.0	0.9	5.9	0.6	6.0	0.9	5.2	0.9				
12°N	6.0	0.8	5.5	0.6	6.0	0.8	5.0	0.7				
9°N	5.7	0.6	5.1	0.5	5.2	0.7	4.9	0.7				
6°N	3.7	0.4	5.0	0.5	5.6	0.6	5.0	1.0	6.0	1.1	5.0	1.4
3°N	4.9	0.4	4.9	0.4	5.7	0.8	5.1	1.2	5.7	1.7	5.2	0.8
0	4.6	0.4	4.6	0.4	5.9	0.8	4.9	1.6	6.0	1.9	5.0	1.5
3°S	3.1	0.5	4.9	0.42	5.6	0.6	5.1	0.75	6.0	1.6	5.0	1.0
6°S	4.9	0.6	5.0	0.45	5.8	0.6	5.75	1.0	6.0	1.1	5.1	1.3
9°S	5.4	0.9	5.0	0.8	5.4	0.5	5.4	0.8	6.0	0.9	6.0	1.0
12°S	6.0	1.1	5.0	1.0	5.5	0.7	5.6	0.7	6.0	1.0	7.0	1.9
15°S	6.0	1.3	5.5	1.1	6.0	1.0	5.8	0.8	6.0	1.0	7.5	1.9
18°S	6.0	1.5	6.0	1.2	6.0	1.4	5.9	0.8	6.0	1.0	7.0	1.8

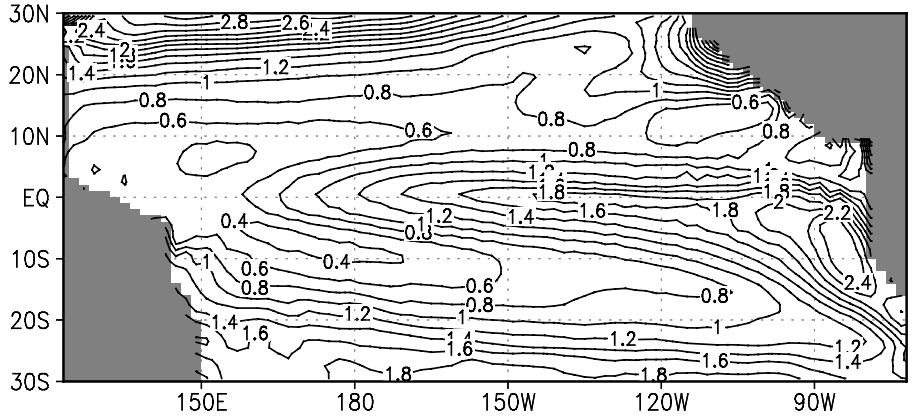

Fig. 4. Distribution of the standard deviations of sea surface temperature computed from model outputs (σ_m). The contour interval is 0.2°C.

become much larger instead. In the region outside of 20°N(S), the zonal correlation scales obviously decrease by contrast with those in the same region at surface.

The meridional correlation scales are all much smaller than those of the zonal direction with values of several hundred kilometers (Fig. 3). The main feature at the surface is that the scales decrease from the equator to both 30°N and 30°S except for the southeast area where the scales are larger along the coast. At a depth of 165 m, however, the trend of the scales almost reverses. The values increase from the equator poleward in the central and west Pacific, but they are large along the American coast off the equator. In the region between 150°W and 120°W, the distribution is complex.

The distribution of standard deviations at the sea surface is shown in Fig. 4, where the large variation extends to the western Pacific along the equator from the South American coast. The results of the computed meridional correlation scales and standard deviations at the sea surface agree well with those by Meyers et al. (1991) based on observed sea surface temperature data in the tropical Pacific. Table 1 gives the averaged meridional scales and standard deviations calculated by Meyers et al. (1991) in the west (New Caledonia–Japan), central (New Caledonia–Hawaii), and east (Tahiti–Panama) Pacific, respectively. For comparison, the corresponding results computed from the model outputs in these regions are also given. Although the values differ somewhat, the trends resemble each other. The root mean square difference of the meridional scales between these two results is 0.6° in latitude, which is only about 70 km in the tropical region. Considering that the results of Meyers et al. (1991) were obtained by averaging the scales in a band and that we only select the values over three definite routes, these two results are quite comparable.

4. Date assimilation experiments

4.1 *Data*

The data type, accuracy, and distribution in space and time govern the quality of the results produced by the data assimilation system. Comparatively, the temperature observations are currently available with sufficient quality for assimilation. In this work, we only perform the assimilation of temperature. The data used in the model and assimilation include SST (Reynolds and Smith, 1994), XBT (expendable bathythermaograph measurements) profiles obtained from a variety of sources, TOGA–TAO array data, and some mooring profiles. To have a consistent surface wind stress product, we also combined the climatological surface wind stress (Hellerman and Rosentein, 1983) and FSU wind stress anomaly (Bourassa et al., 2001). The World Ocean Altas 1998 (WOA98: Conkright et al., 1998) is also used for comparison with the outcome of the experiment.

The temperature profiles were combined at NCEP and passed a standard quality control to remove the bad records, except those from 1982–1998 have not yet received the final stage of the standard quality control. The available data in the tropical Pacific are selected and received further checking, especially for the period from 1982–1989, ensuring that the temperature is not over the land of the model, that the temperature is between 0°C and 32°C, and that it does not contain unrealistic inversions with depth.

Time stepping is carried out using the incremental update method at every day of the model integration. The correction field is created using data within 15 days on either side of the present timestep in a statistical objective analysis scheme. In the assimilation

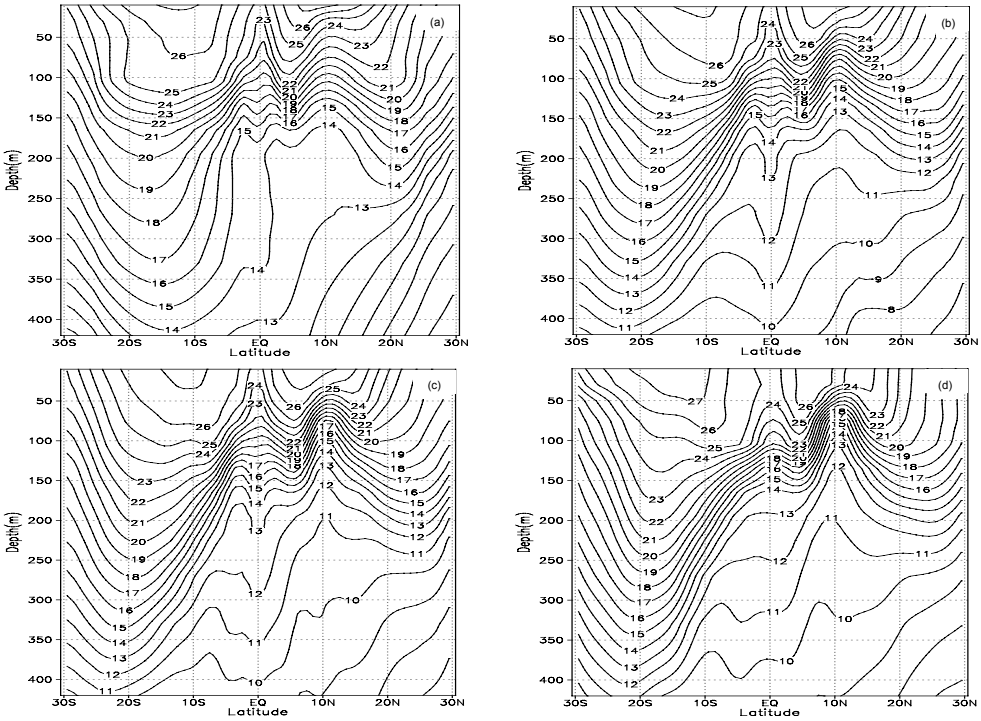

Fig. 5. A latitude-depth cross section along 130°W of annual mean temperature: (a) from the control run, (b) from the previous scheme, (c) from the new scheme, and (d) from WOA98. The contour interval is 1°C.

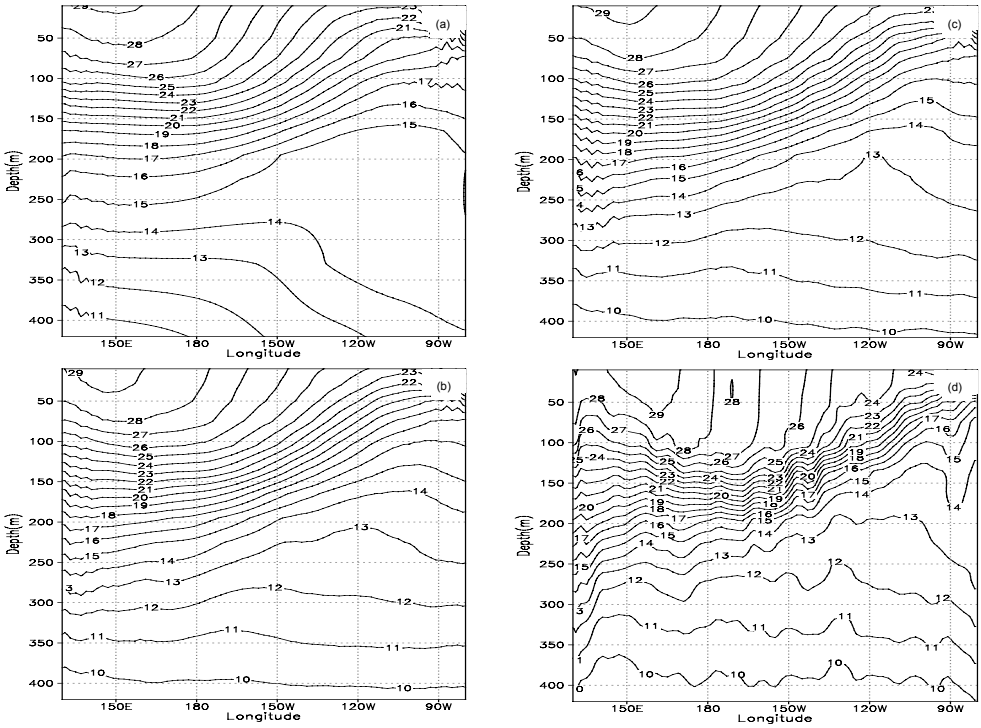

Fig. 6. A longitude-depth cross section along the equator of annual mean temperature: (a) from the control run, (b) from the previous scheme, (c) from the new scheme, and (d) from WOA98. The contour interval is 1°C.

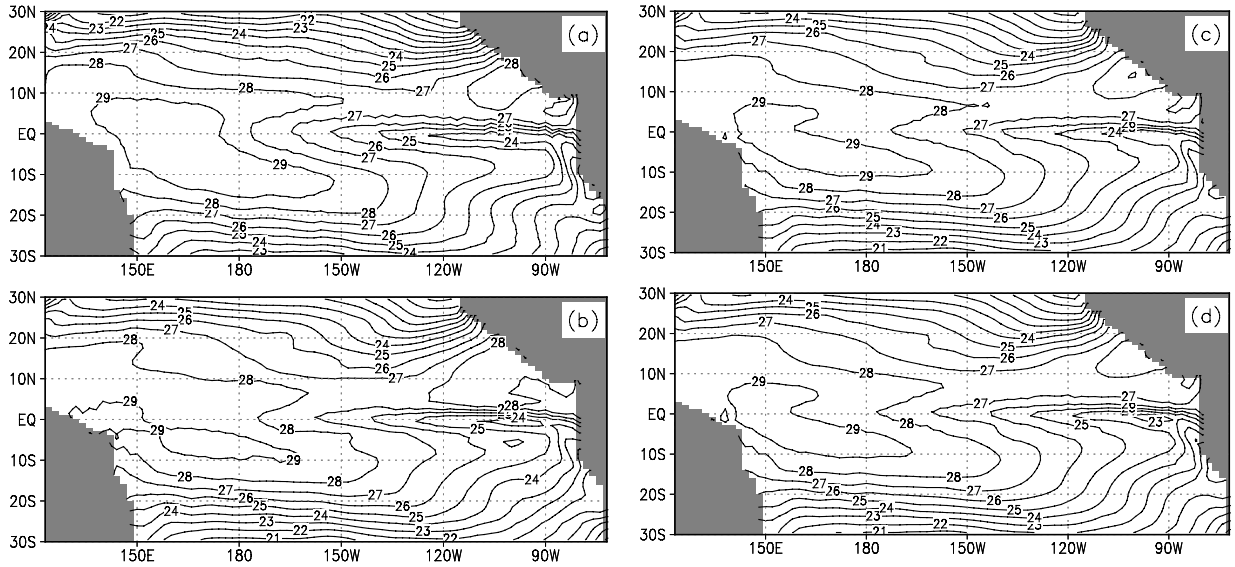

Fig. 7. Distribution of annual mean sea surface temperature: (a) from the control run, (b) from previous scheme, (c) from the new scheme, and (d) from Reynolds and Smith (1994). The contour interval is 1°C.

procedure, the increment is obtained by the preconditioned conjugate gradient algorithm (Navon and Legler, 1987; Deber and Rosati, 1989).

4.2 *Results*

In section 3, we discussed the method to calculate the background error covariance and compared the results with those from observation. But we need to examine to what degree the new estimation can improve the performance. In this section we perform three experiments. The first one is the control run, in which the model is driven only by the wind stress force and heat content from 1978 to 2002, hereafter also referred to as the run without data assimilation. The second experiment starts under the same conditions, but from 1982 the temperature is updated by Optimum Interpolation (OI) with the previous background error covariance scheme (Zhou and Li, 2000). The third one is the same as the second, but with the new estimated background error covariance. The results of the three experiments are compared with observed data, analysis data including WOA98, analyzed SST (Reynolds and Smith, 1994), and TOGA–TAO array data.

In Fig. 5, the latitude-depth profile of annual mean temperature along 130°W is shown. Comparisons for the three experiments and WOA98 show several biases in the results of the model without data assimilation. The most prominent biases are the sparse themocline, the quite warm temperature below the thermocline from north to south, and the improperly curved ridgeline around 17°S. At 10°N, the temperature trough is weaker. After assimilation, the warm temperature in lower levels is corrected greatly and the trough-ridge structure is closer to the observation especially in the third experiment. Figure 6 displays the east-west cross section of annual mean equatorial temperature. The feature of the tropical Pacific is that there is a seasonal, westward-tilted thermocline. The bias of the model's results (experiment one) lies in that that the gradient of the thermocline is weak and the isotherm is sparse. Moreover, at the lower layers of the ocean, the temperature is higher than the analysis data. The assimilation corrects the two biases notably. After assimilation, the isotherms are dense and the gradient of the thermocline better fits that of the observation. The annual mean field indicates that the forecast results are significantly improved after the assimilation. In addition, the new scheme ameliorates the result of experiment two in some areas.

Figure 7 contains the annual mean sea surface temperature from the three experiments and observation. The "warm pool" in the control run is much larger and its position deviates eastward from the observation. The westward cold tongue is weaker. These are greatly corrected after the assimilation. The new scheme modifies the "warm pool" as well as the "warm tongue" near the North American continent.

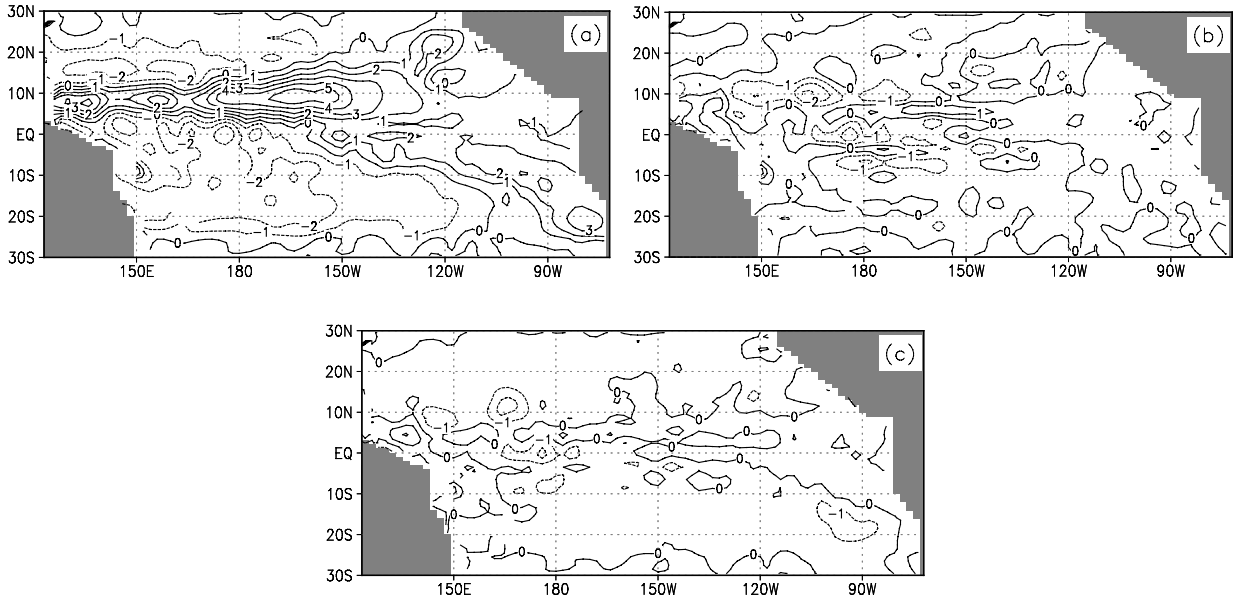

Fig. 8. Difference of monthly mean temperature (March) at 165 m: (a) between model and WOA98, (b) between previous assimilation and WOA98, and (c) between new assimilation and WOA98. The contour interval is 1°C and the dashed line is for negative values.

Figure 8 displays the temperature difference at the level of 165 m in the three experiments. Without assimilation, the obvious biases are the warm temperatures almost entirely in the eastern Pacific. In the northern domain of the equator, there are also warm temperatures with the maximum differences over 4°C in the central Pacific (10°N) for the control run. In most areas of the west/central Pacific south of the equator, the simulated temperatures are lower than those of WOA98. The maximum exceeds 2°C, located at 16°S (Fig. 8a). The previous assimilation scheme (experiment two) reduces the biases in most areas. For example, the warm temperature in the central Pacific near 10°N is evidently corrected and the bias in the eastern Pacific near the equator is also rectified. But in the central Pacific, warm and cold biases of small magnitudes still exist in some areas. With the new scheme, however, some of these areas in which biases occur remarkably disappear. The reason why the temperature without assimilation departs greatly (over 4°C) from the observation in the central/west Pacific north of the equator can possibly be ascribed to: (1) the vertical resolution of the model at the thermocline is too coarse and the pressure gradient due to the gradients of the upper layer thickness do not balance with the pressure gradient due to the wind forcing (Moore and Anderson, 1989); (2) the observation error in this area is large. The problem likewise occurs in other models.

To further the comparison, some TOGA–TAO array profiles are extracted as independent references and not used in the assimilation processes. These TAO profile time series are averaged over a month and are interpolated vertically into the model levels for comparison. Figure 9 shows the vertical profile of temperature in the western Pacific (2°N, 150°E). The unassimilated profiles obviously differ from the observation in the thermocline, where the maximum difference reaches 5°C for the control run. Significant improvements are made by the new assimilation scheme to reduce this bias, and the curve corresponds very well to that of the observation. Figure 10 is similar to Fig. 9, but it shows the eastern equatorial Pacific (0°, 130°W). An obvious temperature difference exists at the surface between the models and the observation. It converges well to the observation with the new scheme, also.

From the above comparisons, we can see the improvement produced by the assimilation on the results of model forecast field. This indicates that the new estimation of background error covariance is an effective and feasible method.

5. Summary and discussion

In this paper, a new estimation of the background error covariance for oceanic data assimilation based on OI is described. In the estimation, the spatial correlation scales and background error variance are acquired primarily from the model output using a novel method.

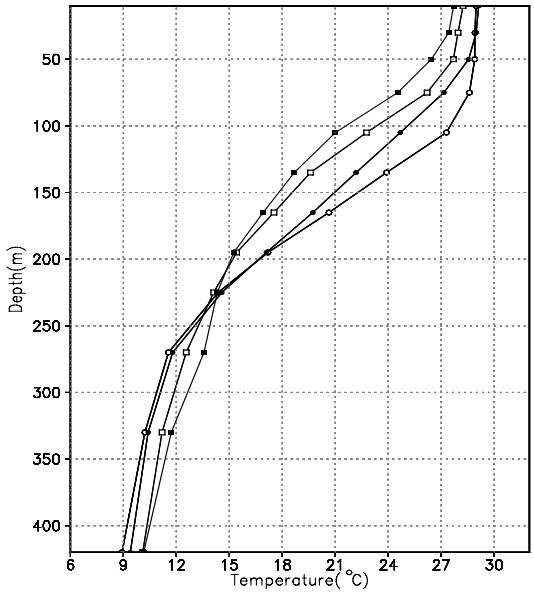

Fig. 9. Profile of monthly mean temperature of March 1987 at (2°N, 150°E). Hollow circles are observation from TOGA–TAO, solid circles are for the new scheme, hollow squares are for the previous scheme, and solid squares are for no assimilation.

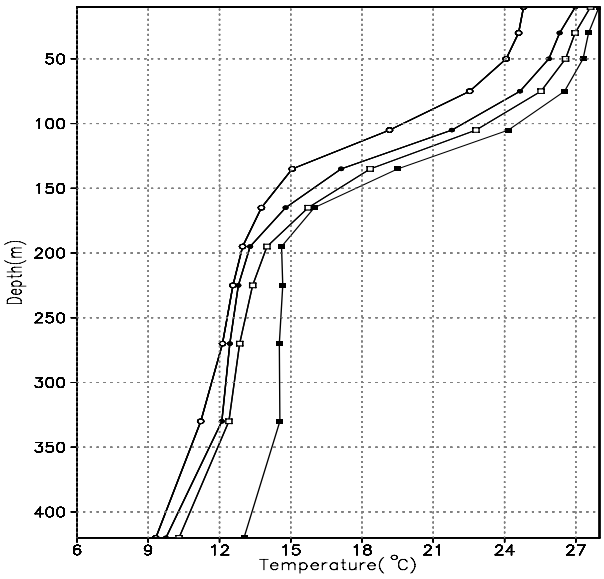

Fig. 10. Same as in Fig. 9, but for January 1987 at (0°, 130°W).

The detailed horizontal structures of the correlation scales in the model space and their variation with depth are obtained; this would be very difficult to do by using observations because of their sparse distribution and discontinuity in time in some areas. The variance for the background error is assumed to be a part of the model simulation, and is estimated from the model results directly. The main features agree well with other studies (Meyers et al., 1991; McPhaden and Taft, 1998) based on observed data. Moreover, we consider the impact of the background field itself in the structure of the covariance which governs the extension of the information in different directions – the anisotropy. Based on the new estimation, three experiments are performed to examine the impact of the estimation. A remarkable improvement in the quality of the model forecasts can be seen clearly after the estimation of background error covariance.

Although positive and effective results are achieved by the new estimation, there is still much to improve. The vertical interaction between model levels and the impact due to time lag on the background error covariance are excluded in the current estimation; these are the focus of our future work. The impact of the background field, i.e. the difference of temperature, introduced in this study is just an experiment to explore the underlying physical correlation structure. It is a simple way to gain the isotropical spatial structure of the background error covariance. More definite physical explainations still remain unknown. The method also has its own limitations. It is easy to envision that in a high-resolution model, the cost of computation is multiplied and more CPU time and memory space will be used. So how to reduce the computation costs is very important for the implementation of the method.

Acknowledgments. We are very grateful to the anonymous reviewers for their critical reading and comments for our manuscript. We also thank Prof. Jiang Zhu of Institute of Atmospheric Physics, Chinese Academy of Sciences for many beneficial discussions. WOA98 data are provided by the NOAA-CIRES Climate Diagnostics Center, Boulder, Colorado, USA, from their Web site at *http://www.cdc.noaa.gov/*. This study is supported by the National Key Program for Developing Basic Sciences (G1999032801), and the National Natural Science Foundation of China (Grant No. 40005007, 40233033, and 40221503).

REFERENCES

Behringer, W., M. Ji, and A. Leetmaa, 1998: An improved coupled model for ENSO prediction and implications

for ocean initialization. Part I: The ocean data assimilation system. *Mon. Wea. Rev.*, **126**, 1013–1021.

Bourassa, M. A., S. R. Smith, and J. J. O'Brien, 2001: A new FSU winds and flux climatology. *11th Conference on Interations of the Sea and Atmosphere*, San Diego, CA, Amer. Meteor. Soc., 912.

Carton, J. A., G. Chepurin, and X. Cao, 2000: A simple ocean data assimilation analysis of the global upper ocean 1950–95. Part I: Methodology. *J. Phys. Oceanogr.*, **30**, 294–309.

Clancy, R. M, P. A. Phoebus, and K. D. Pollak, 1990: An operational global-scale ocean thermal analysis system. *J. Atmos. Ocenanic Technol.*, **7**, 233–254.

Conkright, M., S. Levitus, T. O'Brien, T. Boyer, J. Antonov, and C. Stephens, 1998: *World Ocean Atlas 1998 CD-ROM Data Set Documentation.* Tech. Rep. **15**, NODC Internal Report, Silver Spring, MD. 16pp.

DAO, 1996: Algorithm Theoretical Basis Document 1996 (ATBD). Data Assimilation Office, NASA's Goddard Space Flight Center.

Derber, J., and A. Rosati, 1989: A global oceanic data assimilation system. *J. Phys. Oceanogr.*, **19**, 1333–1347.

Hellerman, S., and M. Rosenstein, 1983: Normal monthly wind stress over the world ocean with error estimates. *J. Phys. Oceanogr.*, **13**, 1093–1104.

Hollingsworth, A., and P. Lonnberg, 1986: The statistical structure of short-range forecast errors as determined from radiosonde data. Part I: The wind field. *Tellus*, **38A**, 111–136.

Levitus, S., 1982: Climatological Altas of the World Ocean. NOAA Prof. Paper, No. 13, U. S. Govt. Printing office, 173pp.

Lorenc, A. C., 1986: Analysis methods for numerical weather prediction. *Quart. J. Roy. Meteor. Soc.*, **112**, 1177–1194.

McPhaden, M. J., and B. A. Taft, 1988: Dynamics of seasonal and intraseasonal variability in the eastern equatorial Pacific. *J. Phys. Oceanogr.*, **18**, 1713–1732.

Meyers, G., H. Phillips, N. Smith, and J. Springtall, 1991: Space and timescales for optimal interpolation of temperature – Tropical Pacific Ocean. *Progress in Oceanography*, **28**, 189–218.

Moore, A, M., and D. L. T. Anderson, 1989: The assimilation of XBT data into a layer model of the tropical Pacific Ocean. *Dyn. Atmos. Oceans,* **13**, 441–464.

Navon, I, M, and D. M. Legler, 1987: Conjugate-gradient methods for large-scale minimization in meteorology. *Mon. Wea. Rev.*, **115**, 1479–1502.

Rabier, F., A. Mcnally, E. Andersson, P. Courtier, P. Unden, J. Eyre, A. Hollingsworth, and F. Bouttier, 1998: The ECMWF implementation of three-dimensional variational assimilation. II: Structure functions. *Quart. J. Roy. Meteor. Soc.*, **124**, 1809–1829.

Reynolds, R. W., and T. M. Smith, 1994: Improved global sea surface temperature analysis. *J. Climate*, **6**, 929–948.

Riishøgaard, L. P., 1998: A direct way of specifying flow-dependent background error correlations for meteorological analysis system. *Tellus*, **50A**, 42–57.

Rosati, A., and K. Miyakoda, 1988: A general circulation model for upper ocean circulation. *J. Phys. Oceanogr.*, **18**, 1601–1626.

Zhang, R-H, and M. Endoh, 1992: A free surface general circulation model for the tropical Pacific Ocean. *J. Geophys. Res.*, **97** (C7), 11237–11255

Zhou Guangqing, and Li Xu, 2000: An oceanic data assimilation system based on a global OGCM. In *Studies on Short-Term Climate Prediction System in China. II: Studies on Dynamical Models for Operational Short-Term Climate Prediction.* China Meteorological Press, Beijing, 393–400. (in Chinese)

Zhou Guangqing, Zeng Qingcun, and Zhang Ronghua, 1999: An improved coupled ocean-atmosphere general circulation model and its numerical simulation. *Progress in Natural Sciences*, **9**, 374–381.

Zhou Guangqing, and Zeng Qingcun, 2001: Predictions of ENSO with a coupled GCM. *Adv. Atmos. Sci.,* **18**, 587–603.

Zhu, J., and M. Kamachi, 2000: An adaptive variational method for data assimilation with imperfect models. *Tellus*, **52A**, 265–279.